JGR Biogeosciences

RESEARCH ARTICLE
10.1029/2024JG008671

Discharge Modulates the Dominance of Downstream Carbon Export Over Evasion in a Boreal Headwater Stream

Demian Hauptmann[1], Marcus Klaus[2], Ryan A. Sponseller[1], Carolina Olid[3], Hjalmar Laudon[2], and Jan Karlsson[1]

[1]Department of Ecology, Environment and Geoscience, Umeå University, Umeå, Sweden, [2]Department of Forest Ecology and Management, Swedish University of Agricultural Sciences, Umeå, Sweden, [3]Department of Earth and Ocean Dynamics, University of Barcelona, UB-Geomodels Research Institute, Barcelona, Spain

Abstract Carbon dioxide (CO_2) evasion and downstream export of carbon (C) from headwater streams represent important fluxes in the global C cycle. Yet, these fluxes are generally studied in isolation, leaving gaps in the understanding of the overall role of streams in the C cycle. In this study, we carried out high resolution measurements of dissolved inorganic and organic C to estimate CO_2 evasion and C export along a 400 m reach of a boreal headwater stream to assess the magnitude and control of the C evasion:export ratio. Higher downstream C export (3.1–74.0 kg C d^{-1}) compared to CO_2 evasion rates (0.53–2.56 kg C d^{-1}) for the full stream network over the open water season resulted in an average C evasion:export ratio of 0.23, which corresponds to a 17% loss of C entering the stream through CO_2 evasion. The temporal variation in C evasion:export ratios (0.03–0.60) was mainly driven by stream discharge, largely through its strong influence on downstream C export. Further, CO_2 evasion showed high spatial variability, and we demonstrate that using only data of a subset of the stream reach would lead to a wide range in the overall C evasion:export ratios upscaled to the whole stream network. Resolving the processes controlling spatial and temporal variation in C fluxes and understanding the importance of discharge for the fate of C routed through streams is crucial for predicting the terrestrial C sink capacity at high latitudes under a changing climate.

Plain Language Summary Streams and rivers are conduits for substantial amounts of carbon from land to atmosphere and from land to ocean. Among freshwaters, headwater streams are particularly important because they evade a disproportionally large amount of CO_2 to the atmosphere despite their relatively small surface area. Headwater streams also transport large amounts of carbon downstream. Despite their importance in the global carbon cycle, the role of streams and rivers as atmospheric sources of CO_2 versus conduits for downstream carbon flux is not well constrained. We therefore conducted a study in a boreal headwater stream and aimed to resolve the relative importance of CO_2 evasion to the atmosphere versus downstream export of carbon. While we found substantial carbon loss through evasion throughout the open water season, the dominant carbon flux was downstream transport. More carbon was shunted downstream during high flow conditions, even when concurrent CO_2 evasion was higher than during base-flow conditions. Discharge was therefore negatively correlated to the overall carbon evasion:export ratio. Climate change is projected to alter precipitation and discharge patterns, and our results demonstrate how such changes may alter the timing and magnitude of carbon routing through headwater streams.

Key Points:

- On average 17% of the carbon entering the stream reach was evaded and 83% exported downstream during the open water season
- Over the open water season, the carbon evasion:export ratio varied from 0.03 to 0.60 and was negatively correlated with discharge
- Not accounting for spatial variability in CO_2 evasion will bias estimates of the carbon evasion:export ratio

Supporting Information:

Supporting Information may be found in the online version of this article.

Correspondence to:

D. Hauptmann,
hauptmann.demian@gmail.com

Citation:

Hauptmann, D., Klaus, M., Sponseller, R. A., Olid, C., Laudon, H., & Karlsson, J. (2026). Discharge modulates the dominance of downstream carbon export over evasion in a boreal headwater stream. *Journal of Geophysical Research: Biogeosciences*, *131*, e2024JG008671. https://doi.org/10.1029/2024JG008671

Received 2 DEC 2024
Accepted 15 DEC 2025

Author Contributions:

Conceptualization: Demian Hauptmann, Marcus Klaus, Ryan A. Sponseller, Carolina Olid, Hjalmar Laudon, Jan Karlsson
Data curation: Demian Hauptmann
Formal analysis: Demian Hauptmann
Funding acquisition: Marcus Klaus, Carolina Olid, Jan Karlsson
Investigation: Demian Hauptmann, Marcus Klaus, Carolina Olid
Methodology: Demian Hauptmann, Marcus Klaus, Ryan A. Sponseller, Carolina Olid, Jan Karlsson
Project administration: Jan Karlsson
Resources: Ryan A. Sponseller, Hjalmar Laudon

1. Introduction

Global freshwaters are conduits for substantial amounts of terrestrial carbon (C) to the atmosphere and the ocean (Battin et al., 2009, 2023; Regnier et al., 2022). Among freshwaters, headwater streams are highly abundant globally (Allen & Pavelsky, 2018) and are particularly important C sources compared to their relatively small surface area (Raymond et al., 2013). Yet, while small streams are hotspots for C loss through carbon dioxide (CO_2) evasion (Li et al., 2021) and downstream export (Downing & Striegl, 2018) there is also uncertainty in their roles within the broader C cycle (Drake et al., 2018; Duvert et al., 2018; Marx et al., 2017). Refined global C flux models (Lauerwald et al., 2023; Raymond et al., 2013) and the addition of streams from often understudied regions (Chiriboga & Borges, 2023; Duvert et al., 2025; Horgby et al., 2019) have advanced our understanding of the magnitude of C fluxes at local and global scales. Despite this progress, studies often focus on individual C fluxes in isolation, for example, either CO_2 evasion or downstream C export, leading to a general lack of data on C evasion to downstream export ratios (Vachon et al., 2023). Further, available studies on C evasion:export ratios

Supervision: Marcus Klaus, Ryan A. Sponseller, Jan Karlsson
Validation: Demian Hauptmann, Carolina Olid
Visualization: Demian Hauptmann
Writing – original draft: Demian Hauptmann
Writing – review & editing: Demian Hauptmann, Marcus Klaus, Ryan A. Sponseller, Carolina Olid, Hjalmar Laudon, Jan Karlsson

are biased towards larger rivers, include uncertainty due to poor spatiotemporal resolution in flux measurements, and lack detailed assessments on the controlling factors for observed major variability (0.37–6.0) in ratios (Argerich et al., 2016; Richey et al., 2002). This knowledge gap limits our ability to understand and quantify the larger role of streams as reactors versus conduits in the C cycle (Cole et al., 2007; Raymond et al., 2016), potentially resulting in biased estimates of the contemporary and future fate of terrestrial C export to aquatic system and the C cycling at landscape level (Karlsson, 2024).

The C evasion:export ratio of headwater catchments is likely to be more dynamic in space and time than in larger rivers. First, this ratio is expected to be sensitive to the strength of land-water connectivity, which is more pronounced in headwaters compared to large streams and rivers (Hotchkiss et al., 2015), and can include a high degree of spatial heterogeneity in the terrestrial supply of dissolved and gaseous C (e.g., Lupon et al., 2019). Second, smaller streams typically have greater hydrological variability than larger rivers, including greater responsiveness to precipitation events (Wood et al., 1990). More dynamic hydrological regimes can lead to greater spatial and temporal variability in the relative supply of different C forms (Gómez-Gener et al., 2021), but also in water residence times and stream thermal regimes (Brown et al., 2005), which may affect the relative importance of in situ processing and aquatic CO_2 production versus evasion of CO_2 externally supplied from soils (Vachon et al., 2023). Thus, while studies on the C evasion:export ratio have attempted to summarize budgets for catchments of varying size (Argerich et al., 2016; Hope et al., 2001; Serikova et al., 2018; Striegl et al., 2012; Wallin et al., 2013), these have not sufficiently constrained the spatial and temporal variability of the C evasion: export ratio.

We therefore estimated the C evasion:export ratio for a boreal headwater stream over the ice-free period and assessed how seasonal changes in hydrology and temperature influence the variability in the balance of these C fates. To address these objectives, we used a combination of temporally and spatially intensive sampling of CO_2 evasion along a 400 m stream reach and compared the average evasion fluxes to concurrent estimates of downstream C export from the stream reach. We also assessed the effect of spatial heterogeneity in CO_2 evasion when estimating the C evasion:export ratio. Our results thus provide an opportunity to explore the potentially dynamic significance of stream CO_2 evasion relative to broader C fluxes from headwater catchments.

2. Materials and Methods

2.1. Study Site

The study was conducted in Torrkälsbäcken, a first-order stream that is part of the research infrastructure Trollberget Experimental Area as part of the Krycklan Catchment Study (Laudon et al., 2021), located northwest of Umeå, northern Sweden (Figure 1). The mean annual temperature measured at the close-by Svartberget research station is 2.1°C (1986–2015) with the lowest temperature in January (−8.6°C), the highest temperature in July (14.6°C), and mean annual precipitation is 619 mm (Laudon et al., 2021).

The stream channel and banks are influenced by historical ditching and straightening that peaked in the region between 1920 and 1930 (Hasselquist et al., 2018). Those ditches are characterized by steep V-shaped banks and straightened channels. While the stream banks still show some of those features (especially the V-shape), the wetted channel is often underfit and the streambed is periodically modified by high discharge events. The stream is characterized by pool-riffle structures with occasional runs and steps, where pools and runs comprise sections with wetted widths of up to 2 m, and the riffle sections average at 30 cm stream width. Average channel slope between sampling stations S1–S18 is 3.1 ± 1.8% (mean ± standard deviation; Figure 2a). The streambed substrate varies from fine sand and organic material in pools and slow-flowing areas to a mixture of small cobbles. The hydrological regime is characterized by rapid, short-term increases in discharge during snow melt between late April and mid-May as well as various rain events during the open-water season (April-October). Base flow usually varies between 0.5 and 2 L^{-1} s^{-1}. Riparian vegetation is dominated by Scots pine (*Pinus sylvestris*), Norway spruce (*Picea abies*), and a few single birch trees (*Betula ssp.*). The forest floor around the stream is dominated by a thick moss layer, including the parts within the V-shaped stream bank that are periodically inundated during storm-events with high discharge.

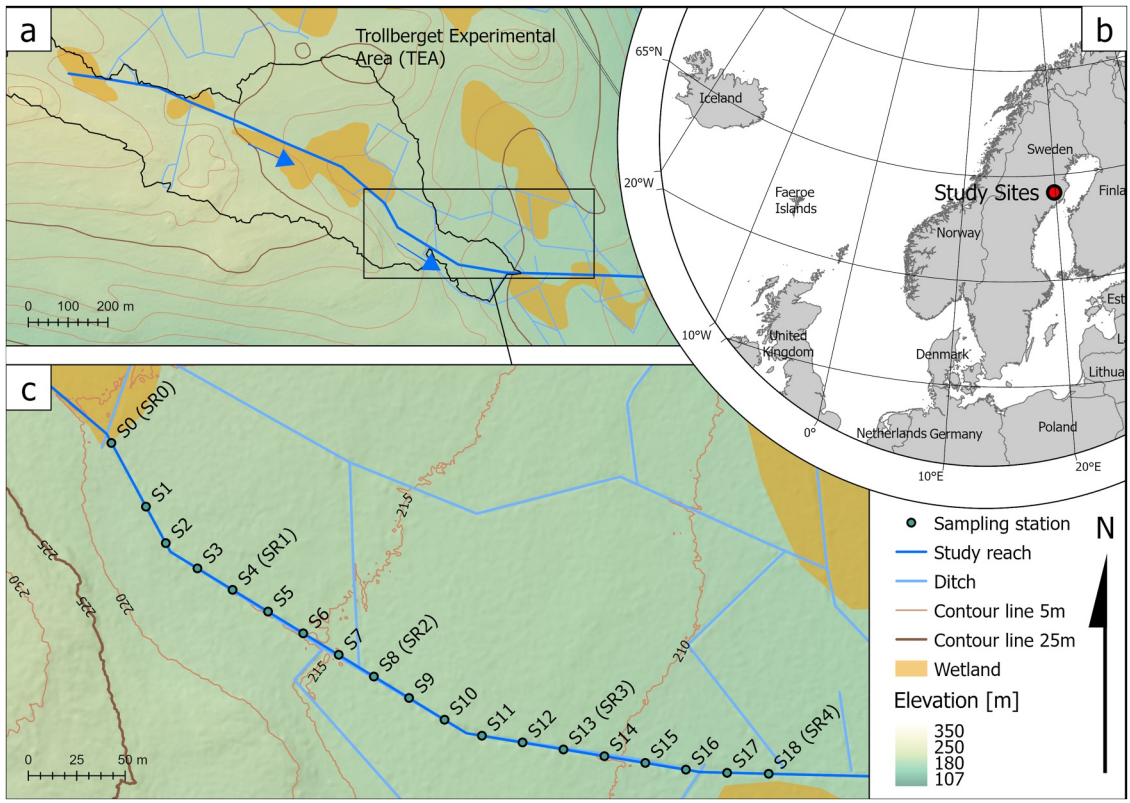

Figure 1. Overview of location of the Trollberget Experimental Area (TEA) (a), relative location within northern Europe (b) and a close-up of the study reach within TEA (c). Manual sampling stations (SX) and continuous sampling stations (SRX) are numbered in ascending order in downstream direction. The wetland surrounding the upper stream reach is highlighted with orange shading. The light blue lines show ditches that were dry during the study period and the dark blue line shows the study reach that retained surface water continuously.

2.2. Setup of Continuous Sampling Stations

We established five continuous sampling stations (SR0, SR1, SR2, SR3, SR4; Figure 1) approximately 100 m apart, covering a total reach length of 400 m (Figure 1). We monitored stream hydrology and chemistry from June to September 2020. At the beginning of the study reach (SR0) we deployed a continuous water level sensor (TruTrack WT-HR 1000; Ipswich, England) in a stilling well with a one-hour logging interval. Additionally, at each station we placed a CO_2 probe wrapped in a semipermeable polytetrafluorethylene membrane (Vaisala GMP252; Vantaa, Finland) on a cinderblock and coupled it to a datalogger (CR300Series; Campbell Scientific Inc., Logan, Utah, United States) with a two-hour sampling interval. Before deployment and upon retrieval, we calibrated the CO_2 probes using a range of known reference gas concentrations (Air Liquide; Paris, France) to cover the expected gradient of CO_2 concentrations (1000, 3000 and 10,000 ppm). Air pressure was measured at a nearby wetland using a pressure-logger (Barologger 5, Solinst ®, Georgetown, Ontario, Canada) with a one-hour sampling interval.

2.3. Setup of Manual Sampling

Between April and September 2020, we sampled every 20 m along the study stream reach, including five continuous sampling stations (SR0–SR4; Figure 1). We collected samples at the 19 sampling stations (S0–S18) but only report 18 measurements per sampling date (S1–S18), because we did not estimate CO_2 evasion or export from S0. We sampled weekly during spring flood in late April to early May and then transitioned to a bi-weekly schedule until the end of the season, for a total of 11 sampling campaigns. On each date, we used a handheld probe (YSI Pro Solo, Xylem Inc., Washington, DC, United States) to measure stream temperature, temperature-specific conductivity (SPC), and air pressure. To measure dissolved inorganic carbon (DIC) and CH_4, we injected 5 mL of bubble-free stream water into a glass vial (flushed with N_2) that was sealed with a butyl rubber septum. The vial was prefilled with 20 µL of 4% HCl to preserve the sample and to shift the carbonate system to CO_2. Stream water

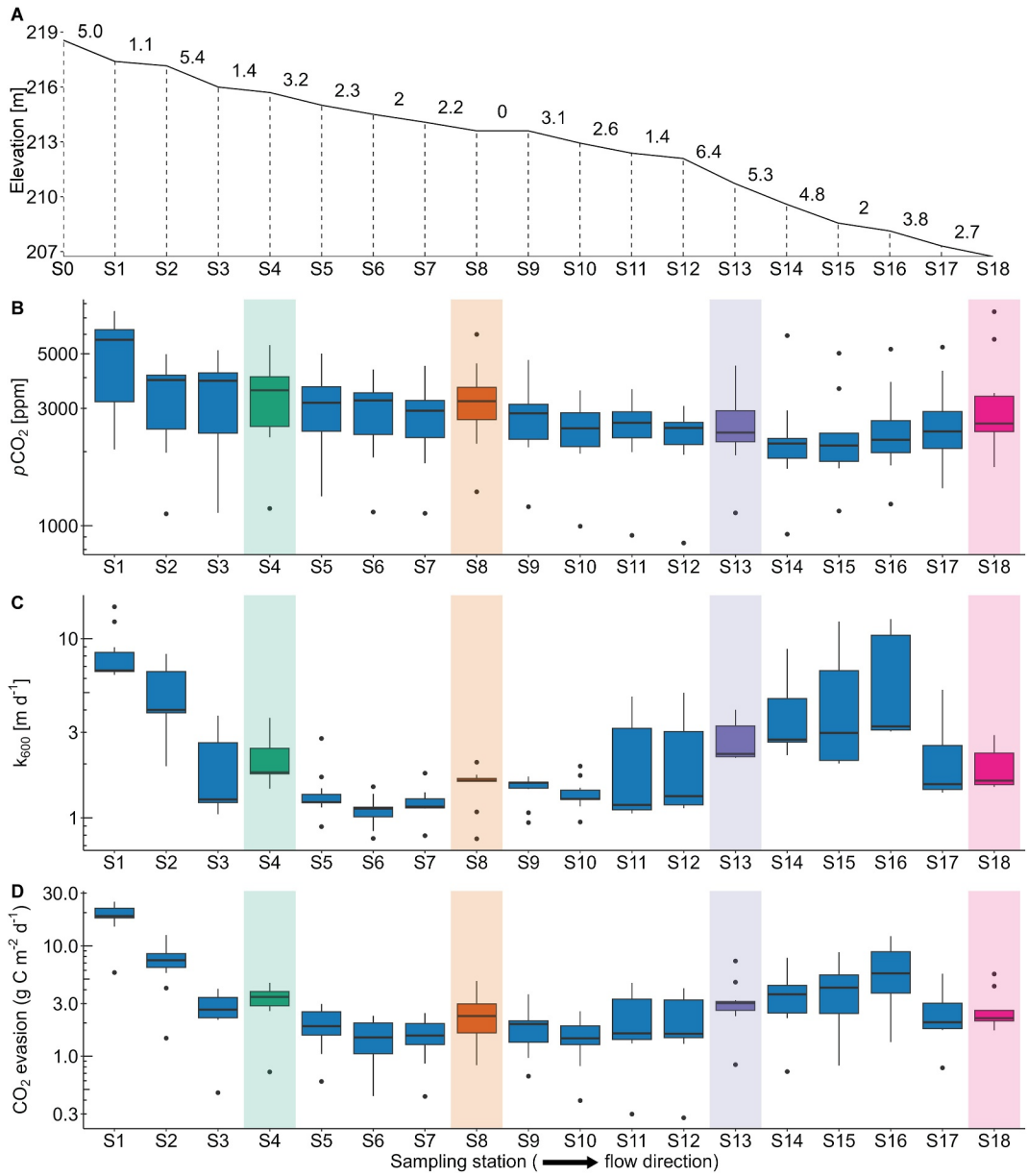

Figure 2. Longitudinal profile of sampling stations, where (a) shows elevation of each sampling station and the channel slope (%) for each segment (e.g., S0-S1, S1-S2 etc.). Panels (b)–(d) show boxplots along a spatial gradient along the *x*-axis (station in downstream order) and the temporal variation along the *y*-axis for (b) pCO_2, (c) gas exchange velocity (k_{600}) and (d) CO_2 evasion along the study reach between April and September. Stations are named S1–S18, and continuous stations are colored in green (SR1 = S4), orange (SR2 = S8), purple (SR3 = S13) and pink (SR4 = S18). Boxplots show the inner quartile range, thick horizontal lines denote median, whiskers represent 1.5 times inner quartile range, and dots denote outliers.

samples for dissolved organic carbon (DOC) and nutrients were collected in acid-washed high-density polyethylene bottles, transported in a cooling box and stored at 4°C before filtration (0.45 µm; Sarstedt, Filtropur S) in the lab. Samples were also collected without headspace for immediate analysis of pH.

2.4. Chemical Analyses

DIC was determined from the vial headspace pCO_2, analyzed using a gas chromatograph with a flame ionization detector (Clarus 580, PerkinElmer, Shelton, CT, USA) and a headspace sampler (TurboMatrix 110, PerkinElmer, Shelton, CT, USA). Headspace CH_4 concentrations were measured from the same samples. Samples for DOC and

total dissolved nitrogen were stored at 4°C and analyzed within 10 days after sampling using the combustion catalytic oxidation method on a TOC VCPH analyzer (Shimadzu, Duisburg, Germany). Filtered samples for soluble reactive phosphorous (SRP) and dissolved inorganic nitrogen (DIN) species were stored at −18°C before analysis on an Autoanalyzer AA3 (Omniprocess AB, Solna, Sweden) following method No. G-297-04 for phosphate ($P\text{-}PO_4$), method No. G-171-96 for ammonium ($N\text{-}NH_4$) and method No. G-384-08 for nitrate ($N\text{-}NO_3$). We measured pH on a benchtop meter (Mettler Delta 340) with a pH Sensor (InLab® Power electrode, Mettler Toledo, Columbus, Ohio, United States).

2.5. Flux Calculations and Gas Exchange Velocity k_{600}

We calculated air-water CO_2 fluxes (F_{CO_2}, g C m^{-2} d^{-1}) using Fick's first law of diffusion as:

$$F_{CO_2} = k_{CO_2} \times K_H \times M_C \times p \times \left(pCO_{2,water} - pCO_{2,air}\right) \times p_{conv.} \quad (1)$$

where K_H is the Henry constant (mol L^{-1} atm^{-1}), expressing temperature-specific gas solubility in water, calculated according to (Wanninkhof, 2014), k_{CO_2} is the temperature- and CO_2 specific gas exchange velocity (m d^{-1}), M_C is the molar mass of carbon (12.011 g C mol^{-1}), p is air pressure (mbar), $pCO_{2,air}$ and $pCO_{2,water}$ is the partial pressure of CO_2 (ppm) in the atmosphere and the water, respectively and $p_{conv.}$ is a unit conversion factor (0.9869×10^{-3} atm $mbar^{-1} \times 10^3$ L $m^{-3} \times 10^{-6}$) to account for pressure, volume and ppm conversions. We assumed $pCO_{2,air} = 414$ ppm and corrected $pCO_{2,water}$ readings for probe-specific influences by temperature, air pressure and water depth (Johnson et al., 2010). For the manual samples, we calculated CO_2 from DIC using stream water pH and temperature following standard carbonate equilibrium equations (Stumm & Morgan, 1996). We found that CO_2 on average made up 98.2 ± 0.7% of the DIC pool.

We estimated the standardized gas exchange velocity for CO_2 at 20°C (k_{600}) at each stream reach based on ambient sound recordings (Klaus et al., 2019). We used a stereo handheld audio recorder (Tascam DR-05X, TEAC Corporation, Santa Fe Springs, CA, USA) and recorded ambient sound 30 cm above the stream surface during minimal noise disturbance (e.g., avoided human sounds or airplanes). We inferred k_{600} from signatures in the sound pressure level spectrum that are caused by air entrainment (bubbles) in riffles and steps (see Klaus et al., 2019). We calculated the temperature-specific gas exchange velocity for CO_2 (k_{CO_2}):

$$k_{CO_2} = \left(\frac{Sc_{CO_2}}{600}\right)^{-0.5} \times k_{600} \quad (2)$$

where Sc_{CO_2} is the gas and temperature specific Schmidt number following Wanninkhof (2014).

2.6. Continuous Discharge and Gas Exchange Velocity

We established a rating curve to generate continuous estimates of discharge along the stream reach and then used these estimates to model continuous k_{600}. Our rating curve was constructed from 23 direct estimates of discharge determined from dilution gauging (i.e., salt slugs; Moore, 2004) at station SR0. From these, we characterized the relationship between stage and discharge using the lm() function with ln-transformed discharge and ln-transformed stage height in R (version 4.1.0; R Core Team, 2021). The model outputs (Intercept and Slope) were used in a power law (Figure S1 in Supporting Information S1; $R^2 = 0.83$, $p < 0.001$, $n = 23$):

$$y = a \times x^b \quad (3)$$

where a is exp(intercept) and b is the slope. We additionally used the manual salt-slug measurements at stations SR1–SR4 to estimate the downstream increase in discharge from ordinary least squares (OLS) regression between adjacent sampling stations (i.e., SR0-SR1, SR1-SR2, SR2-SR3, SR3-SR4; $n = 23$ April 2020 to October 2022, Figure S2 in Supporting Information S1). To obtain continuous k_{600} at SR1–SR4, we used OLS of manually recorded discharge and k_{600} from a total of 18 sampling campaigns (between April 2020 and October 2022) and applied the resulting equation to our continuous discharge estimates (Figure S3 in Supporting Information S1). We did not take concurrent (manual) discharge measurements for the manual sampling stations (Figure 1; S1–S18), and therefore assumed a linear increase in discharge between the stations with continuous loggers

(SR0–SR4). We estimated k_{600} for the manual sampling stations using a combination of individual k_{600} estimates from audio recordings during the first four sampling occasions (30/04, 07/05, 20/05 and 04/06) while for the later samplings for which audio recordings were missing (18/06, 02/07, 16/07, 30/07, 13/08, 26/08 and 10/09) we used estimates from OLS of Q and k_{600} (Figure S4 in Supporting Information S1) at every sampling location (Figure 1) from the 18 sampling campaigns between April 2020 and October 2022.

2.7. Calculating the C Evasion:Export Ratio

We multiplied the average C evasion rate by stream area to yield an estimate of whole-stream CO_2 evasion. To estimate stream area, we determined channel length for the full stream length using existing geographic data (Lidberg et al., 2017) and assumed that channel width was equivalent to the average of each of the study reaches. We estimated average CO_2 evasion from the stream (g C d^{-1}) as:

$$F_{CO_{2,stream}} = w_{avg.} \times L \times F_{CO_{2,station}} \quad (4)$$

where $w_{avg.}$ is average stream width (m), L is stream length (m) and $F_{CO_{2,station}}$ is CO_2 evasion (g C m^{-2} d^{-1}) averaged from 4 to 18 stations. While the stream length was measured using GIS (Section 2.9) and assumed static, width was measured at every station during the sampling visits and therefore reflects the dynamic variability during different discharge conditions. Further, we re-visited the study stream during the tenth of July 2025 (Figure S5 in Supporting Information S1) and recorded complementary measurements of stream width, pCO_2 and k_{600} (Figure S6 in Supporting Information S1). The re-visit happened during a dry period, which resulted in reduced water levels, stream width and especially k_{600}. The resulting data does however support our assumption, that stream width is similar upstream from our study reach (Table S1, Figure S6 in Supporting Information S1). Downstream C export (g C d^{-1}) was calculated by multiplying discharge by the concentration of the different carbon species (DOC and CO_2) at the end of the reach (g C d^{-1}):

$$C\ \text{export} = Q \times (c\text{DOC} + c\text{CO}_2) \quad (5)$$

where Q is discharge (L d^{-1}), cDOC is DOC concentration (g C L^{-1}) and cCO_2 is CO_2 concentration (g C L^{-1}). The CH_4 concentrations were very low (0.02% CO_2 concentration) and therefore assumed negligible to the overall C fluxes. We did not account for POC given that previous work in this region indicates that particles contribute <0.6% to the stream water C pool (Laudon et al., 2011). To estimate the C evasion:export ratio for the whole stream (ALL), we used the average CO_2 evasion rate and area for all stations S1–S18, scaled it to the whole stream length and divided it by the C export from S18. To account for the potential sensitivity of spatial variability in CO_2 evasion, we generated four different estimates of the C evasion:export ratio, following the same approach as above but separately using the average CO_2 evasion rate and area for each of the four sub-reaches and the C export calculated from each of the "outlets" of the sub-reaches (SR1–SR4). The C evasion:export ratio expresses the relationship of CO_2 evasion to downstream export of carbon species, which in this study are dominated by DIC and DOC. When the ratio is between 0 and 1.0, more C was exported in downstream direction than lost through CO_2 evasion, and the stream acts mostly as conduit. A ratio above 1.0 expresses a surplus of CO_2 evasion relative to export and that the study system is losing more C to the atmosphere than through aquatic export, which indicates that the stream is functioning primarily as a reactor.

2.8. Statistical Analyses

To validate whether CO_2 evasion calculated from grab samples followed a similar distribution as CO_2 evasion from continuous loggers, we used Kolmogorov–Smirnov and Kuiper's tests correcting for autocorrelation (Lanzante, 2021) after verifying temporal autocorrelation using a Durbin-Watson test from the R package "lmtest" ($p < 0.001$). We tested for linear relationships between C export and Q, the C evasion:export ratio and temperature, as well as the C evasion:export ratio and Q for each of the four sub-reaches using $\log_{10}$-transformed variables and OLS using the lm() function. We then used the intercepts of the linear model between the C evasion: export ratio and discharge and regressed them against the average C evasion per sub-reach using the lm() function. We used OLS to test how discharge was related to reach scale CO_2 evasion. Additionally, we used OLS to test how channel slope relates to the temporal variation of k_{600} expressed as the coefficient of variation (CV) of k_{600}

for the 18 manual sampling sites. All calculations and analyses were conducted using R (version 4.1.0; R Core Team, 2021).

2.9. GIS Analysis

We calculated channel slope as the elevation change every 20 m along the study reach (Figure S7 in Supporting Information S1). The 20 m distance is based on the distance between each manual sampling station (Table S2 in Supporting Information S1, e.g. S0-S1, S1-S2). In ArcGIS Pro, we extracted elevation for each of these points and each sampling station from a 0.5 m resolution digital elevation model (DEM, © Lantmäteriet) and measured stream distance along a stream-polyline digitized according to (Lidberg et al., 2017). We then divided distance between the points by elevation change to calculate channel slope. While the 0.5 m DEM allowed relatively accurate stream delineation and slope calculations between stations, it did not resolve microscale bathymetric features such as meandering within the straightened channel, undercut streambanks, steps and plunge pools.

2.10. Error Propagation for C Evasion:Export Ratio

We estimated the error for the C evasion:export ratio estimates for whole stream upscaling scenario (ALL) following the standard rules of error propagation. To yield the absolute error of the evasion component of the ratio, we calculated the error of the mean CO_2 evasion across all 18 stations and the error of the mean width measurements along the study reach (as described in Section 2.7). We calculated with an error of 0 for stream length, because we assumed static stream length. For the export component, we used the measurement error of DOC and CO_2, as well as the standard error of the residuals of the rating curve (Section 2.6) for Q. Lastly, we calculated the absolute error for the C evasion:export ratio and report both, absolute and relative error (Table S3 in Supporting Information S1).

3. Results

3.1. Environmental Variables and Stream Chemistry

Stream water temperature varied from 0.7°C in late April to 11.3°C in late July (Table S4 in Supporting Information S1, Figure 3a) and was on average 7.3 ± 3.5°C (mean ± standard deviation). Generally, water temperatures decreased slightly from SR0 through SR4 with a maximum difference in temperature along the reach of 1.7°C (Table S4 in Supporting Information S1, Figure 3a). Discharge during the grab sampling campaigns ranged from 0.8 to 35.3 L s^{-1} at the upstream station SR0, and 1.1–41.9 L s^{-1} at the downstream station SR4 (Table S4 in Supporting Information S1, Figure 3a). Average discharge at SR0 was 12.7 ± 11.5 L s^{-1} and increased downstream to 17.9 ± 15.2 L s^{-1} at SR4. pH was on average 4.7 ± 0.2 (Table S4 in Supporting Information S1; SR4) across all sampling dates. The concentration of DOC (26.3 ± 8.0 mg L^{-1}) was on average 12-fold higher than that of DIC (1.9 ± 0.9 mg L^{-1}). The average concentrations of DIN ($N\text{-}NH_4$ + $N\text{-}NO_3$) and SRP were 24.2 ± 12.0 and 2.4 ± 0.9 µg L^{-1}, respectively.

3.2. pCO_2 From Grab Samples Over Time and Space

All sample stations along the study reach were consistently supersaturated in CO_2 (average: 2984 ± 1278 ppm; coefficient of variation, CV = 0.43) relative to the atmosphere. The station closest to the upstream wetland had the highest pCO_2 (Figure 2a, S1; 5067 ± 1915 ppm, CV = 0.38) and this was followed by a rapid (~1700 ppm) decrease to S2, located 80 m from the wetland (Figures 2a, 3385 ± 1192 ppm, CV = 0.35). After this, pCO_2 decreased more gradually in a downstream direction before increasing only slightly (~570 ppm) at the very end of the study reach (Figure 2a, S18; 3332 ± 1825 ppm, CV = 0.55). The lowest pCO_2 values (1262 ± 405 ppm) were found in September, one day following a rain event when discharge had already recovered to baseflow conditions (1.39 ± 0.13 L s^{-1}). This outlier is also apparent from the concentration-discharge relationship for DIC (Figure S8 in Supporting Information S1).

3.3. Gas Exchange Velocity (k_{600}) Over Time and Space

The gas exchange velocity k_{600} showed distinct spatial and temporal patterns, with an average for the reach of 2.8 ± 2.6 m d^{-1} (CV = 0.90). The highest average k_{600} were found at the most upstream station associated with a 25 cm high waterfall (Figure 2c; S1; 8.2 ± 2.9 m d^{-1}) and near the end of the reach at another, smaller step

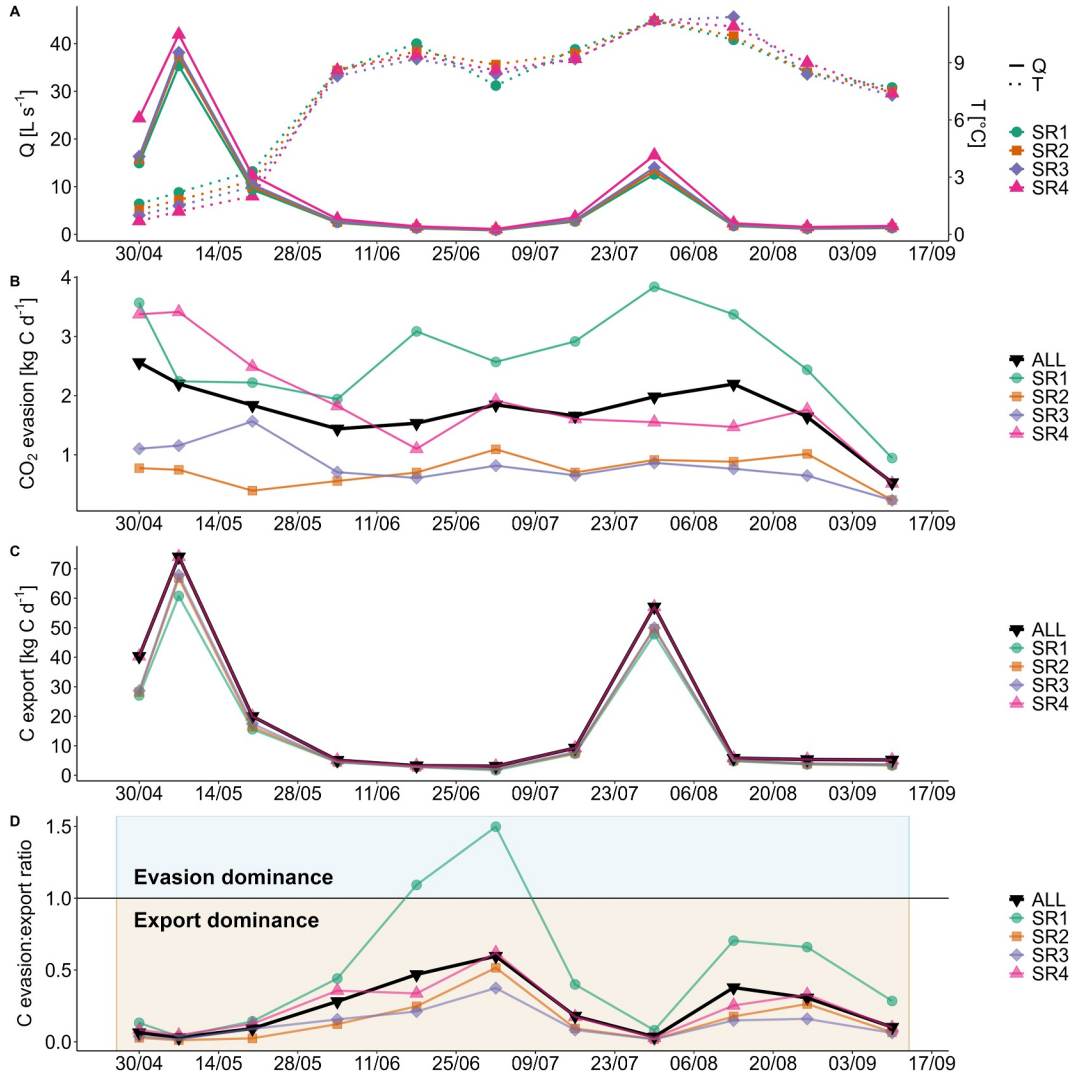

Figure 3. Variation of (a) discharge and temperature, (b) CO_2 evasion, (c) carbon export (dissolved inorganic carbon and dissolved organic carbon export), and (d) carbon evasion:export ratio across the sampling season between April and September. The horizontal line in panel (d) shows the threshold, where evasion and export are equal. Below this line proportionally more C is lost through export and above more C is lost through evasion. ALL is the scenario integrating all sampling stations. Reach length for each assumption (Panel b–d, SR1–SR4 and All) is measured from spring to outlet of the respective reach (see Figure 1). The data underlying this figure are available in Table S5 in Supporting Information S1.

(Figure 2c; S16, 6.3 ± 4.3 m d^{-1}). After that, k_{600} decreased to station S5 (Figure 2c; 1.4 ± 0.5 m d^{-1}) and increased again after station S10 (Figure 2c; 1.4 ± 0.3 m d^{-1}) until S16 (Figure 2c). Between station S5 and S10, k_{600} varied less over space and time compared to the other stations, which had up to a 10.4 m d^{-1} difference between the lowest and highest estimates. k_{600} at the continuous stations (Figure 2, colored shading) was less variable (1.1–3.0 m d^{-1}, CV = 0.22) over time and space than for the grab sampling stations (0.9–9.1 m d^{-1}, CV = 0.71). The coefficient of determination (R^2) of the linear regression between k_{600} and discharge for stations S1 to S18 was on average 0.43 (CV = 0.50), with the lowest fit at S16 (R^2 = 0.14, Figure S4P in Supporting Information S1) and the best fit at S4 (R^2 = 0.79, Figure S4D in Supporting Information S1). Finally, the average k_{600} per sampling station was positively correlated to channel slope; however, this relationship was non-significant when including all stations (Figure S9A in Supporting Information S1, p = 0.27). After excluding outliers (S1, S2 and S16) where cook's distance was greater than three times the mean, we observed a significant, albeit subtle correlation between slope and k_{600} (Figure S9B in Supporting Information S1, R^2 = 0.33; p = 0.03).

We can attribute these outlier stations to their pronounced step profile, which promotes locally higher k_{600} than the slope, averaged over 20 m section length, would suggest.

3.4. CO_2 Evasion Over Time and Space

Average CO_2 evasion from grab samples was 3.8 ± 4.3 g C m^{-2} d^{-1} (CV = 1.11) and varied 12-fold along the study reach. CO_2 evasion was consistently highest at S1 (Figure 2d; 18.7 ± 5.6 g C m^{-2} d^{-1}), was 2-fold lower 20 m further downstream (S2; 7.2 ± 2.8 g C m^{-2} d^{-1}) but tended to be lowest at S6 (Figure 2d; 1.5 ± 0.6 g C m^{-2} d^{-1}). CO_2 evasion rates estimated from logger data were 2.4 ± 1.0 g C m^{-2} d^{-1} and had a higher temporal, but lower spatial variability, compared to grab samples (Figure S10 in Supporting Information S1). However, the overall distribution of CO_2 evasion estimates from grab samples was not significantly different from that derived from continuous logger data and is hence representative for the sampling season (Figure S11 in Supporting Information S1; $p < 0.05$, Kolmogorov–Smirnov and Kuiper's tests). Similar to k_{600}, CO_2 evasion was also positively correlated with channel slope if the same outliers as for k_{600} are removed (Figure S12 in Supporting Information S1, $p = 0.03$).

3.5. Reach Scale CO_2 Evasion and Downstream C Export

On average reach scale CO_2 evasion in the "ALL" scenario represented 17% of all recorded C fluxes and 83% of C was transported in downstream direction. Reach scale CO_2 evasion was highest for SR1 during most of the sampling season (2.7 ± 0.8 kg C d^{-1}). Evasion for SR2 and SR3 was three times lower than for SR1 and varied less over time, indicated by two-times lower standard deviations (Figure 3b; SR2: 0.7 ± 0.3 kg C d^{-1}; SR3: 0.8 ± 0.4 kg C d^{-1}). Evasion for SR4 had similar temporal variation as SR1, but lower values on average (Figure 3b; 1.9 ± 0.9 kg C d^{-1}). Conversely, we found the highest C export rates furthest downstream, during elevated discharge like spring flood (Figure 3c; 74.0 kg C d^{-1}; SR4) and a rain event (Figure 3c; 57.1 kg C d^{-1}; SR4). Despite variation in DOC concentrations across stations (Figure S13 in Supporting Information S1), the magnitude of Q was more important in shaping downstream dynamics of C export. The proportion of DOC to DIC at the end of each sub-reach contributing to export was on average 13:1. Throughout the sampling season, we found evidence for dilution for both DOC and DIC as discharge increased (Figures S8 and S14 in Supporting Information S1). In general, variability in C export over time was to a large degree related to discharge (OLS, $p < 0.001$). Similarly, average reach-scale CO_2 evasion was positively related to discharge over time, but this relationship was not statistically strong (OLS, $p = 0.13$). The same analysis for reaches SR1–SR4 showed that the influence of discharge on CO_2 evasion became stronger in downstream direction (OLS, $p_{SR1} = 0.77$, $p_{SR4} = 0.003$). We also found that C export was negatively related to water temperature (OLS, $p = 0.03$), but also that discharge was negatively correlated with temperature, and that downstream C export was lowest during times where temperature was highest (Figure S15 in Supporting Information S1, OLS, $p = 0.01$).

3.6. C Evasion:Export Ratio and Mechanisms

The C evasion:export ratio was on average 0.23 and varied notably over time (Figure 3d). For example, the two flood events with the highest C export (Figure 3c) resulted in the lowest (0.01) C evasion:export ratio during the study period. By comparison, the C evasion:export ratio was highest (up to 1.5) in early July. The C evasion:export ratio showed a strong negative relationship with discharge (Figure 4a, OLS, $p < 0.002$) and a weak negative relationship with temperature ($R^2 = 0.35$, $p = 0.05$) and the DOC:DIC ratio ($p = 0.02$ to $p = 0.19$; Figure S16 in Supporting Information S1). The latter reflects that DOC primarily contributes to carbon export, while DIC, dominated by CO_2, drives evasion. At higher discharge, DIC is diluted more strongly than DOC (Figures S8, S14 in Supporting Information S1), increasing the DOC:DIC ratio and favoring export over evasion. Despite the positive relationship of k_{600} and discharge (Figure S4 in Supporting Information S1), the dilution effect on DIC overcompensates for the increase in k_{600}, resulting in reduced CO_2 evasion during high flow events.

The sensitivity analysis showed that ignoring spatial variability in C evasion resulted in a range (average 0.12 to 0.50) of C evasion:export ratios, but a similar slope of the relationship to discharge. The uncertainty introduced by variability in C evasion was most apparent during low flow periods, that is, the period when C export was relatively low and variability in CO_2 evasion had a larger overall effect on the ratio. For example, during summer low flow (2020-07-02) upscaling based on C evasion rates from SR1 (Figure 3d; SR1 = 1.50) yielded a more than three times higher C evasion:export ratio than upscaling based on SR3 (Figure 3d; SR3 = 0.37).

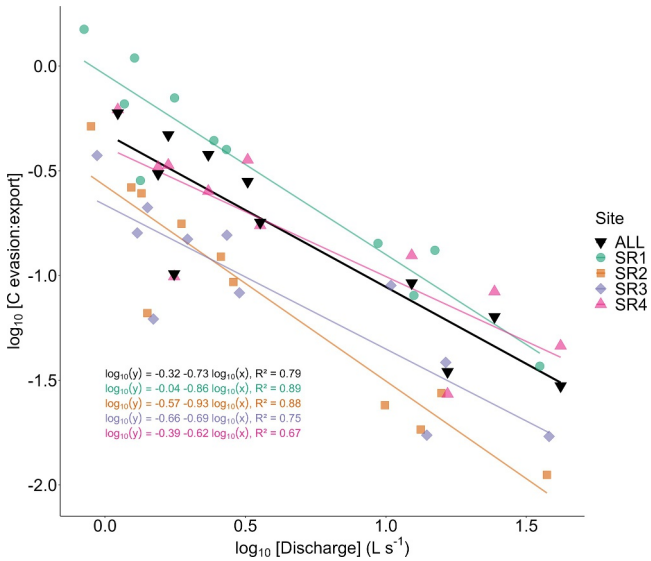

Figure 4. Relationships between C evasion:export ratio and discharge, displayed on $\log_{10}$-scale ($p < 0.002$, for details see Table S6 in Supporting Information S1). Regressions lines and equations, as well as fits are presented for the four different assumptions (SR1–SR4) and the scenario integrating the 18 stations (ALL).

4. Discussion

Boreal streams are known to support high rates of CO_2 evasion (Campeau et al., 2014; Striegl et al., 2012; Wallin et al., 2018) and downstream C export (Aitkenhead & McDowell, 2000), but the balance of these fates remains poorly constrained. Compared to larger rivers, where the C evasion:export ratio ranged from 1 to 6 (Richey et al., 2002; Serikova et al., 2018; Striegl et al., 2012), our headwater stream yielded an average C evasion:export ratio (0.23) close to estimates reported for a temperate, second-order stream catchment (0.37; (Argerich et al., 2016), a Scottish first-order stream (0.52; Hope et al., 2001) as well as to modeled estimates from Canadian watersheds with varying size, but a similar channel slope range as our study (0.20–0.80; (Hutchins et al., 2020). We acknowledge that annual C evasion:export ratios may differ slightly from the numbers reported here, because we are missing data from the winter season when ice and snow cover may limit CO_2 evasion (Clow et al., 2021), and when downstream C fluxes may also be low (Gomez-Gener et al., 2021). Regardless, our results provide detailed information regarding C losses from a single stream across a range of flow conditions. We found that the stream was mainly a conduit, rather than a reactor of carbon and that the extent of these C pathways varied over time. We provide insights into the magnitude of the C evasion:export ratio, its controls over time and how these estimates are influenced by assumptions regarding CO_2 evasion at network scales.

4.1. Spatial and Temporal Patterns of CO_2 Evasion

Throughout the sampling season, this stream reach was strongly supersaturated with CO_2 relative to the atmosphere, and CO_2 concentrations and evasion rates were largely representative of Swedish boreal headwater streams that are (partially) draining wetlands (Klaus et al., 2018; M. Wallin et al., 2010; M. B. Wallin et al., 2013). Yet our estimates incorporated considerable spatial heterogeneity within the study reach. Indeed, despite the relatively small spatial extent of sampling (400 m), we observed as much as a 12-fold difference in average CO_2 evasion rate among individual sampling stations. Similarly, we found up to 6-fold variation in k_{600} during baseflow conditions. CO_2 concentrations and evasion generally showed similar temporal patterns across stations, and rates typically decreased with longitudinal distance from the upstream wetland (mire), which are known to be major sources of CO_2 to streams in northern landscapes (Hope et al., 2001; M. Wallin et al., 2010; M. B. Wallin et al., 2013). Despite the general trend of a decreasing wetland effect on CO_2, we saw increases in CO_2 concentrations in the lower part of the study reach, potentially indicating increased groundwater input promoted by terrain flattening at the hill footslope (Lupon et al., 2019). Further, even smaller-scale spatial heterogeneity in CO_2 evasion emerged along the reach, in part related to changes in channel slope (Figure S9 in Supporting Information S1), but also to very localized morphological features (e.g., plunge pools) that can promote C gas losses (Botter et al., 2022), but remained unresolved in our bathymetric analysis.

Superimposed on spatial patterns were notable temporal changes in CO_2 evasion throughout the open water season, with the five different reach-scale estimates varying by as much as 6-fold across sampling dates. Reach-averaged CO_2 evasion was weakly correlated with discharge, partly via effects of discharge on k_{600} (Figure S4 in Supporting Information S1), which is in agreement with studies on the control over CO_2 evasion elsewhere (Botter et al., 2022; McDowell & Johnson, 2018; Schelker et al., 2016). There was further evidence that temporal patterns of CO_2 evasion varied across our sampling stations within the reach based on local morphology. For example, the mid-section of our reach, which was characterized by wider runs and pools, showed less variability in k_{600} (CV = 0.29) and evasion (CV = 0.48) compared to sections with steps and plunge pools in the upper and lower end of the study reach (CV = 0.88 and 0.74). This pattern likely reflects an interaction between hydrology and geomorphology, where fluctuations in discharge in some locations translate to greater temporal variability in k_{600} (Botter et al., 2022). Taken together, our results are consistent with a growing body of literature highlighting the high degree of temporal and spatial variability in C evasion from streams (Botter et al., 2022; Liu et al., 2022; Rocher-Ros et al., 2019).

4.2. Downstream C Export

Similar to C evasion, the magnitude of downstream export of C (DIC + DOC) was strongly linked to variation in discharge. DOC concentrations were on average 13-fold higher than DIC concentrations, which is also in agreement with observations made from other boreal headwaters (Gómez-Gener et al., 2021; Tank et al., 2018). Further, during high discharge events, there was clear evidence for dilution of DOC and especially DIC concentrations, suggesting supply limitation of both C forms (Creed et al., 2015; Knapp et al., 2020). Such a pattern is common for boreal streams draining open mires, which, compared to forest hillslopes, tend to support more preferential flow paths that bypass soils and thus strongly dilute solutes, particularly during snowmelt (Laudon et al., 2011). Yet, despite this overarching seasonal pattern, we also observed the highest DOC concentrations during a rain event in late July (Figure S13 in Supporting Information S1). This event appeared to mobilize DOC, through activation of humus-rich riparian soil layers (Ledesma et al., 2018), but had the opposite (diluting) effect on stream DIC. Opposing relationships between discharge and DOC and DIC are common in boreal streams (Gómez-Gener et al., 2021; Rehn et al., 2022), as well as differences in stream chemistry responses to snowmelt versus summer floods (Gomez-Gener et al., 2021), but both can make it more complex to disentangle patterns of C export in headwater streams with highly variable discharge patterns.

4.3. Carbon Evasion:Export Ratios

The C evasion:export ratio varied over time, and temporal variability was largely explained by a negative relationship with discharge. This pattern could reflect the overwhelming influence of discharge on external C loading and downstream export, but could also indicate a loss in the capacity for instream CO_2 production and gas exchange as water transit time decreases (Serikova et al., 2018). These mechanisms are not mutually exclusive, and we are unable to resolve them with the current data. Yet, other studies in boreal headwater streams indicate that external CO_2 supply far surpasses internal CO_2 production from mineralization of organic C (Lupon et al., 2019; Winterdahl et al., 2016).

Although the C evasion:export ratios for the different upscaling assumptions all varied over time with discharge, the magnitude of the ratio was sensitive to our assumptions of the areal CO_2 evasion rate (Figure 4). This influence was notably apparent during low and base flow conditions, when the C evasion:export ratio varied by as much as 0.37 to 1.50 across our different scenarios. This variation largely results from applying different aerial CO_2 evasion rates averaged over the different sub-reaches to the entire upstream network, the implications of which are amplified during low flow periods when the longitudinal C fluxes are weak. During high flow conditions however, the assumptions regarding CO_2 evasion were less important, as the longitudinal C export rates overwhelmed the C evasion:export ratio, thereby reducing the variation in the ratio to 0.01–0.05. Regardless, these results highlight the importance to account for the spatial variability in CO_2 evasion for estimating accurate C evasion:export ratio.

Our results offer additional insights of the controls and patterns of the fate of terrestrial C in running waters. Work on larger systems have suggested an overall importance of hydrological travel times for the fate of land C to evasion versus export (Algesten et al., 2004; Hotchkiss et al., 2015; Serikova et al., 2018). For example, based on latitudinal patterns of high C evasion:export ratios in rivers with long transit times in West Siberian lowlands, and comparison of ratios with other higher order systems, Serikova et al. (2018) suggested that the relative fate of land C export to evasion versus downstream export is largely controlled by water transit times through its effect on time for mineralization and outgassing within the river networks. Our results of lower C evasion:export within a headwater stream in response to seasonal increases in discharge support the overwhelming influence of hydrological transit times for these C fates. Thus, both spatial variability in C evasion:export across stream reaches and systems, as well as temporal patterns in C evasion:export within systems, can be assumed to be largely affected by variation in travel times. Although not studied here, the magnitude and patterns in C evasion:export ratios with hydrological transit time also likely differ depending on regional differences in for example, speciation and quality of the terrestrial C supply (Striegl et al., 2012; Vachon et al., 2023), including balance between organic and inorganic inputs as well as the quality of organic matter and alkalinity (Raymond & Hamilton, 2018). We acknowledge the need for systematic temporal assessments of C evasion and export across streams and rivers of various orders to advance the understanding of the contemporary and future fate of land C in running waters.

5. Conclusions

Overall, our results show significant temporal and spatial variability in C evasion and export along a 400 m stream reach. Specifically, our findings illustrate how discharge regulates the magnitude of the C evasion:export ratio and how coverage of spatial heterogeneity in stream C evasion affect evasion:export ratios. We show that overall, our study system operates as a significant conduit for downstream C transport while also evading significant amounts of CO_2. This finding has important implications for the transport of C from land to oceans and in particular the length of loops that cycle C between terrestrial ecosystems, inland waters and the atmosphere (Regnier et al., 2022). In particular, our results and the comparison with literature data highlight how the length of these loops can be site-specific and dynamic over time. Discharge modulates terrestrial C input to streams (Rehn et al., 2022; Riml et al., 2019) and with higher discharge, a larger proportion of terrestrial gross primary production is exported from land and partially evaded to the atmosphere in streams and rivers (Liu et al., 2022; Öquist et al., 2014). Our study highlights the need of partitioning the land C loss into their various fates for a holistic understanding of landscape C budget responses to discharge (Vachon et al., 2020). The results imply that during periods with higher discharge, relatively more of the C in headwater streams could potentially circumvent evasion through possible uptake and/or burial in downstream systems. In contrast, during low discharge there is a higher chance for immediate loss through evasion higher up in the catchment. Larger-scale studies that account for all possible fates of C across the aquatic continuum are needed to assess the role of hydrology for the length of land-to-ocean C loops (Liu et al., 2022; Regnier et al., 2022). Such assessments are of particular importance in the light of climate change scenarios that suggest substantial future changes in precipitation and discharge regimes of many streams and rivers globally (IPCC, 2023; van Vliet et al., 2013).

Conflict of Interest

The authors declare no conflicts of interest relevant to this study.

Data Availability Statement

The data used for analysis is openly available at the Data repository ZENODO (https://doi.org/10.5281/zenodo.18201309) with CC BY 4.0 licensing.

Acknowledgments
We thank Erik Geibrink, Jenny Ekman, Jonas Lundholm, Abdulmajid Mahomoud and Meredith Blackburn for lab- and field help and the Biogeochemical Analytical Facility (BAF) at Umeå university for chemical analysis. We thank the two anonymous reviewers and the editors whose comments and suggestions improved this paper. This study was supported by FORMAS (Grant 2018-00885), Stiftelsen Skogssällskapet (Grant 2019-657-Steg 2 2018) and FORMAS (Grant 2018-01217).

References

Aitkenhead, J. A., & McDowell, W. H. (2000). Soil C:N ratio as a predictor of annual riverine DOC flux at local and global scales. *Global Biogeochemical Cycles*, *14*(1), 127–138. https://doi.org/10.1029/1999GB900083

Algesten, G., Sobek, S., Bergström, A.-K., Ågren, A., Tranvik, L. J., & Jansson, M. (2004). Role of lakes for organic carbon cycling in the boreal zone. *Global Change Biology*, *10*(1), 141–147. https://doi.org/10.1111/j.1365-2486.2003.00721.x

Allen, G. H., & Pavelsky, T. M. (2018). Global extent of rivers and streams. *Science*, *361*(6402), 585–588. https://doi.org/10.1126/science.aat0636

Argerich, A., Haggerty, R., Johnson, S. L., Wondzell, S. M., Dosch, N., Corson-Rikert, H., et al. (2016). Comprehensive multiyear carbon budget of a temperate headwater stream. *Journal of Geophysical Research: Biogeosciences*, *121*(5), 1306–1315. https://doi.org/10.1002/2015JG003050

Battin, T. J., Lauerwald, R., Bernhardt, E. S., Bertuzzo, E., Gener, L. G., Hall, R. O., et al. (2023). River ecosystem metabolism and carbon biogeochemistry in a changing world. *Nature*, *613*(7944), 449–459. https://doi.org/10.1038/s41586-022-05500-8

Battin, T. J., Luyssaert, S., Kaplan, L. A., Aufdenkampe, A. K., Richter, A., & Tranvik, L. J. (2009). The boundless carbon cycle. *Nature Geoscience*, *2*(9), 598–600. https://doi.org/10.1038/ngeo618

Botter, G., Carozzani, A., Peruzzo, P., & Durighetto, N. (2022). Steps dominate gas evasion from a mountain headwater stream. *Nature Communications*, *13*(1), 7803. https://doi.org/10.1038/s41467-022-35552-3

Brown, L. E., Hannah, D. M., & Milner, A. M. (2005). Spatial and temporal water column and streambed temperature dynamics within an alpine catchment: Implications for benthic communities. *Hydrological Processes*, *19*(8), 1585–1610. https://doi.org/10.1002/hyp.5590

Campeau, A., Lapierre, J.-F., Vachon, D., & del Giorgio, P. A. (2014). Regional contribution of CO_2 and CH_4 fluxes from the fluvial network in a lowland boreal landscape of Québec. *Global Biogeochemical Cycles*, *28*(1), 57–69. https://doi.org/10.1002/2013GB004685

Chiriboga, G., & Borges, A. V. (2023). Andean headwater and piedmont streams are hot spots of carbon dioxide and methane emissions in the Amazon basin. *Communications Earth & Environment*, *4*(1), 76. https://doi.org/10.1038/s43247-023-00745-1

Clow, D. W., Striegl, R. G., & Dornblaser, M. M. (2021). Spatiotemporal dynamics of CO_2 gas exchange from headwater Mountain streams. *Journal of Geophysical Research: Biogeosciences*, *126*(9), e2021JG006509. https://doi.org/10.1029/2021JG006509

Cole, J. J., Prairie, Y. T., Caraco, N. F., McDowell, W. H., Tranvik, L. J., Striegl, R. G., et al. (2007). Plumbing the global carbon cycle: Integrating inland waters into the terrestrial carbon budget. *Ecosystems*, *10*(1), 172–185. https://doi.org/10.1007/s10021-006-9013-8

Creed, I. F., McKnight, D. M., Pellerin, B. A., Green, M. B., Bergamaschi, B. A., Aiken, G. R., et al. (2015). The river as a chemostat: Fresh perspectives on dissolved organic matter flowing down the river continuum. *Canadian Journal of Fisheries and Aquatic Sciences*, *72*(8), 1272–1285. https://doi.org/10.1139/cjfas-2014-0400

Downing, J. A., & Striegl, R. G. (2018). Size, age, renewal, and discharge of groundwater carbon. *Inland Waters*, *8*(1), 122–127. https://doi.org/10.1080/20442041.2017.1412918

Drake, T. W., Raymond, P. A., & Spencer, R. G. M. (2018). Terrestrial carbon inputs to inland waters: A current synthesis of estimates and uncertainty. *Limnology and Oceanography Letters*, *3*(3), 132–142. https://doi.org/10.1002/lol2.10055

Duvert, C., Borges, A. V., Calamita, E., Rocher-Ros, G., Linkhorst, A., Rosentreter, J. A., et al. (2025). Hydroclimate and landscape diversity drive highly variable greenhouse gas emissions from tropical and subtropical inland waters. *Nature Water*, *3*(11), 1303–1317. https://doi.org/10.1038/s44221-025-00522-8

Duvert, C., Butman, D. E., Marx, A., Ribolzi, O., & Hutley, L. B. (2018). CO_2 evasion along streams driven by groundwater inputs and geomorphic controls. *Nature Geoscience*, *11*(11), 813–818. https://doi.org/10.1038/s41561-018-0245-y

Gómez-Gener, L., Hotchkiss, E. R., Laudon, H., & Sponseller, R. A. (2021). Integrating discharge-concentration dynamics across carbon forms in a boreal landscape. *Water Resources Research*, *57*(8), e2020WR028806. https://doi.org/10.1029/2020WR028806

Hasselquist, E. M., Lidberg, W., Sponseller, R. A., Ågren, A., & Laudon, H. (2018). Identifying and assessing the potential hydrological function of past artificial forest drainage. *Ambio*, *47*(5), 546–556. https://doi.org/10.1007/s13280-017-0984-9

Hope, D., Palmer, S. M., Billett, M. F., & Dawson, J. J. C. (2001). Carbon dioxide and methane evasion from a temperate peatland stream. *Limnology & Oceanography*, *46*(4), 847–857. https://doi.org/10.4319/lo.2001.46.4.0847

Horgby, Å., Segatto, P. L., Bertuzzo, E., Lauerwald, R., Lehner, B., Ulseth, A. J., et al. (2019). Unexpected large evasion fluxes of carbon dioxide from turbulent streams draining the world's mountains. *Nature Communications*, *10*(1), 4888. https://doi.org/10.1038/s41467-019-12905-z

Hotchkiss, E. R., Hall Jr, R. O., Sponseller, R. A., Butman, D., Klaminder, J., Laudon, H., et al. (2015). Sources of and processes controlling CO_2 emissions change with the size of streams and rivers. *Nature Geoscience*, *8*(9), 696–699. https://doi.org/10.1038/ngeo2507

Hutchins, R. H. S., Casas-Ruiz, J. P., Prairie, Y. T., & del Giorgio, P. A. (2020). Magnitude and drivers of integrated fluvial network greenhouse gas emissions across the boreal landscape in Québec. *Water Research*, *173*, 115556. https://doi.org/10.1016/j.watres.2020.115556

IPCC. (2023). Climate Change 2023: Synthesis Report. In H. Lee & J. Romero (Eds.), *Contribution of working groups I, II and III to the sixth assessment report of the intergovernmental Panel on climate change [core writing team* (pp. 35–115). IPCC. https://doi.org/10.59327/IPCC/AR6-9789291691647

Johnson, M. S., Billett, M. F., Dinsmore, K. J., Wallin, M., Dyson, K. E., & Jassal, R. S. (2010). Direct and continuous measurement of dissolved carbon dioxide in freshwater aquatic systems—Method and applications. *Ecohydrology*, *3*(1), 68–78. https://doi.org/10.1002/eco.95

Karlsson, J. (2024). Emergent responses shape the coupled carbon cycle in a changing Arctic. *Nature Water*, *2*(6), 500–501. https://doi.org/10.1038/s44221-024-00250-5

Klaus, M., Geibrink, E., Hotchkiss, E. R., & Karlsson, J. (2019). Listening to air–water gas exchange in running waters. *Limnology and Oceanography: Methods*, *17*(7), 395–414. https://doi.org/10.1002/lom3.10321

Klaus, M., Geibrink, E., Jonsson, A., Bergström, A. K., Bastviken, D., Laudon, H., et al. (2018). Greenhouse gas emissions from boreal inland waters unchanged after forest harvesting. *Biogeosciences*, *15*(18), 5575–5594. https://doi.org/10.5194/bg-15-5575-2018

Knapp, J. L. A., von Freyberg, J., Studer, B., Kiewiet, L., & Kirchner, J. W. (2020). Concentration–discharge relationships vary among hydrological events, reflecting differences in event characteristics. *Hydrology and Earth System Sciences*, *24*(5), 2561–2576. https://doi.org/10.5194/hess-24-2561-2020

Lanzante, J. R. (2021). Testing for differences between two distributions in the presence of serial correlation using the Kolmogorov–Smirnov and Kuiper's tests. *International Journal of Climatology*, *41*(14), 6314–6323. https://doi.org/10.1002/joc.7196

Laudon, H., Berggren, M., Ågren, A., Buffam, I., Bishop, K., Grabs, T., et al. (2011). Patterns and dynamics of Dissolved Organic Carbon (DOC) in boreal streams: The role of processes, connectivity, and scaling. *Ecosystems*, *14*(6), 880–893. https://doi.org/10.1007/s10021-011-9452-8

Laudon, H., Hasselquist, E. M., Peichl, M., Lindgren, K., Sponseller, R., Lidman, F., et al. (2021). Northern landscapes in transition: Evidence, approach and ways forward using the Krycklan Catchment Study. *Hydrological Processes*, *35*(4), e14170. https://doi.org/10.1002/hyp.14170

Lauerwald, R., Allen, G. H., Deemer, B. R., Liu, S., Maavara, T., Raymond, P., et al. (2023). Inland water greenhouse gas budgets for RECCAP2: 1. State-Of-The-Art of global scale assessments. *Global Biogeochemical Cycles*, *37*(5), e2022GB007657. https://doi.org/10.1029/2022GB007657

Ledesma, J. L. J., Kothawala, D. N., Bastviken, P., Maehder, S., Grabs, T., & Futter, M. N. (2018). Stream dissolved organic matter composition reflects the riparian zone, not upslope soils in boreal forest headwaters. *Water Resources Research*, *54*(6), 3896–3912. https://doi.org/10.1029/2017wr021793

Li, M., Peng, C., Zhang, K., Xu, L., Wang, J., Yang, Y., et al. (2021). Headwater stream ecosystem: An important source of greenhouse gases to the atmosphere. *Water Research*, *190*, 116738. https://doi.org/10.1016/j.watres.2020.116738

Lidberg, W., Nilsson, M., Lundmark, T., & Ågren, A. M. (2017). Evaluating preprocessing methods of digital elevation models for hydrological modelling. *Hydrological Processes*, *31*(26), 4660–4668. https://doi.org/10.1002/hyp.11385

Liu, S., Kuhn, C., Amatulli, G., Aho, K., Butman, D. E., Allen, G. H., et al. (2022). The importance of hydrology in routing terrestrial carbon to the atmosphere via global streams and rivers. *Proceedings of the National Academy of Sciences*, *119*(11), e2106322119. https://doi.org/10.1073/pnas.2106322119

Lupon, A., Denfeld, B. A., Laudon, H., Leach, J., Karlsson, J., & Sponseller, R. A. (2019). Groundwater inflows control patterns and sources of greenhouse gas emissions from streams. *Limnology & Oceanography*, *64*(4), 1545–1557. https://doi.org/10.1002/lno.11134

Marx, A., Dusek, J., Jankovec, J., Sanda, M., Vogel, T., van Geldern, R., et al. (2017). A review of CO_2 and associated carbon dynamics in headwater streams: A global perspective. *Reviews of Geophysics*, *55*(2), 560–585. https://doi.org/10.1002/2016RG000547

McDowell, M. J., & Johnson, M. S. (2018). Gas transfer velocities evaluated using carbon dioxide as a tracer show high streamflow to be a major driver of total CO_2 evasion flux for a headwater stream. *Journal of Geophysical Research: Biogeosciences*, *123*(7), 2183–2197. https://doi.org/10.1029/2018JG004388

Moore, R. (2004). Introduction to salt dilution gauging for streamflow measurement part 2: Constant-rate injection. *Streamline Watershed Management Bulletin*, *8*(1), 11–15.

Öquist, M. G., Bishop, K., Grelle, A., Klemedtsson, L., Köhler, S. J., Laudon, H., et al. (2014). The full annual carbon balance of boreal forests is highly sensitive to precipitation. *Environmental Science and Technology Letters*, *1*(7), 315–319. https://doi.org/10.1021/ez500169j

Raymond, P. A., & Hamilton, S. K. (2018). Anthropogenic influences on riverine fluxes of dissolved inorganic carbon to the oceans. *Limnology and Oceanography Letters*, *3*(3), 143–155. https://doi.org/10.1002/lol2.10069

Raymond, P. A., Hartmann, J., Lauerwald, R., Sobek, S., McDonald, C., Hoover, M., et al. (2013). Global carbon dioxide emissions from inland waters. *Nature*, *503*(7476), 355–359. https://doi.org/10.1038/nature12760

Raymond, P. A., Saiers, J. E., & Sobczak, W. V. (2016). Hydrological and biogeochemical controls on watershed dissolved organic matter transport: Pulse-shunt concept. *Ecology*, *97*(1), 5–16. https://doi.org/10.1890/14-1684.1

R Core Team. (2021). *R: A language and environment for statistical computing*. R Foundation for Statistical Computing. Retrieved from https://www.R-project.org/

Regnier, P., Resplandy, L., Najjar, R. G., & Ciais, P. (2022). The land-to-ocean loops of the global carbon cycle. *Nature*, *603*(7901), 401–410. https://doi.org/10.1038/s41586-021-04339-9

Rehn, L., Sponseller, R. A., Laudon, H., & Wallin, M. B. (2022). Long-term changes in dissolved inorganic carbon across boreal streams caused by altered hydrology. *Limnology & Oceanography*, *68*(2), 409–423. https://doi.org/10.1002/lno.12282

Richey, J. E., Melack, J. M., Aufdenkampe, A. K., Ballester, V. M., & Hess, L. L. (2002). Outgassing from Amazonian rivers and wetlands as a large tropical source of atmospheric CO_2. *Nature*, *416*(6881), 617–620. https://doi.org/10.1038/416617a

Riml, J., Campeau, A., Bishop, K., & Wallin, M. B. (2019). Spectral decomposition reveals new perspectives on CO_2 concentration patterns and soil-stream linkages. *Journal of Geophysical Research: Biogeosciences*, *124*(10), 3039–3056. https://doi.org/10.1029/2018JG004981

Rocher-Ros, G., Sponseller, R. A., Lidberg, W., Mörth, C.-M., & Giesler, R. (2019). Landscape process domains drive patterns of CO_2 evasion from river networks. *Limnology and Oceanography Letters*, *4*(4), 87–95. https://doi.org/10.1002/lol2.10108

Schelker, J., Singer, G. A., Ulseth, A. J., Hengsberger, S., & Battin, T. J. (2016). CO_2 evasion from a steep, high gradient stream network: Importance of seasonal and diurnal variation in aquatic pCO_2 and gas transfer. *Limnology & Oceanography*, *61*(5), 1826–1838. https://doi.org/10.1002/lno.10339

Serikova, S., Pokrovsky, O. S., Ala-Aho, P., Kazantsev, V., Kirpotin, S. N., Kopysov, S. G., et al. (2018). High riverine CO_2 emissions at the permafrost boundary of Western Siberia. *Nature Geoscience*, *11*(11), 825–829. https://doi.org/10.1038/s41561-018-0218-1

Striegl, R. G., Dornblaser, M. M., McDonald, C. P., Rover, J. A., & Stets, E. G. (2012). Carbon dioxide and methane emissions from the Yukon River system. *Global Biogeochemical Cycles*, *26*(4). https://doi.org/10.1029/2012GB004306

Stumm, W., & Morgan, J. J. (1996). *Aquatic chemistry: Chemical equilibria and rates in natural waters* (3rd ed.). Wiley.

Tank, S. E., Fellman, J. B., Hood, E., & Kritzberg, E. S. (2018). Beyond respiration: Controls on lateral carbon fluxes across the terrestrial-aquatic interface. *Limnology and Oceanography Letters*, *3*(3), 76–88. https://doi.org/10.1002/lol2.10065

Vachon, D., Sadro, S., Bogard, M. J., Lapierre, J.-F., Baulch, H. M., Rusak, J. A., et al. (2020). Paired O_2–CO_2 measurements provide emergent insights into aquatic ecosystem function. *Limnology and Oceanography Letters*, *5*(4), 287–294. https://doi.org/10.1002/lol2.10135

Vachon, D., Sponseller, R. A., Rosvall, M., & Karlsson, J. (2023). Controls on terrestrial carbon fluxes in simulated networks of connected streams and Lakes. *Global Biogeochemical Cycles*, *37*(3), e2022GB007597. https://doi.org/10.1029/2022GB007597

van Vliet, M. T. H., Franssen, W. H. P., Yearsley, J. R., Ludwig, F., Haddeland, I., Lettenmaier, D. P., & Kabat, P. (2013). Global river discharge and water temperature under climate change. *Global Environmental Change*, *23*(2), 450–464. https://doi.org/10.1016/j.gloenvcha.2012.11.002

Wallin, M., Buffam, I., Öquist, M., Laudon, H., & Bishop, K. (2010). Temporal and spatial variability of dissolved inorganic carbon in a boreal stream network: Concentrations and downstream fluxes. *Journal of Geophysical Research*, *115*(G2). https://doi.org/10.1029/2009jg001100

Wallin, M. B., Campeau, A., Audet, J., Bastviken, D., Bishop, K., Kokic, J., et al. (2018). Carbon dioxide and methane emissions of Swedish low-order streams—a national estimate and lessons learnt from more than a decade of observations. *Limnology and Oceanography Letters*, *3*(3), 156–167. https://doi.org/10.1002/lol2.10061

Wallin, M. B., Grabs, T., Buffam, I., Laudon, H., Ågren, A., Öquist, M. G., & Bishop, K. (2013). Evasion of CO_2 from streams – The dominant component of the carbon export through the aquatic conduit in a boreal landscape. *Global Change Biology*, *19*(3), 785–797. https://doi.org/10.1111/gcb.12083

Wanninkhof, R. (2014). Relationship between wind speed and gas exchange over the ocean revisited. *Limnology and Oceanography: Methods*, *12*(6), 351–362. https://doi.org/10.4319/lom.2014.12.351

Winterdahl, M., Wallin, M. B., Karlsen, R. H., Laudon, H., Öquist, M., & Lyon, S. W. (2016). Decoupling of carbon dioxide and dissolved organic carbon in boreal headwater streams. *Journal of Geophysical Research: Biogeosciences*, *121*(10), 2630–2651. https://doi.org/10.1002/2016JG003420

Wood, E. F., Sivapalan, M., & Beven, K. (1990). Similarity and scale in catchment storm response. *Reviews of Geophysics*, *28*(1), 1–18. https://doi.org/10.1029/RG028i001p00001